AIP Applied Physics Letters

Surface-bound-exciton emission associated with domain interfaces in m-plane ZnO films

C. C. Kuo, B. H. Lin, Song Yang, W. R. Liu, W. F. Hsieh, and C.-H. Hsu

Citation: Applied Physics Letters **101**, 011901 (2012); doi: 10.1063/1.4732140
View online: http://dx.doi.org/10.1063/1.4732140
View Table of Contents: http://scitation.aip.org/content/aip/journal/apl/101/1?ver=pdfcov
Published by the AIP Publishing

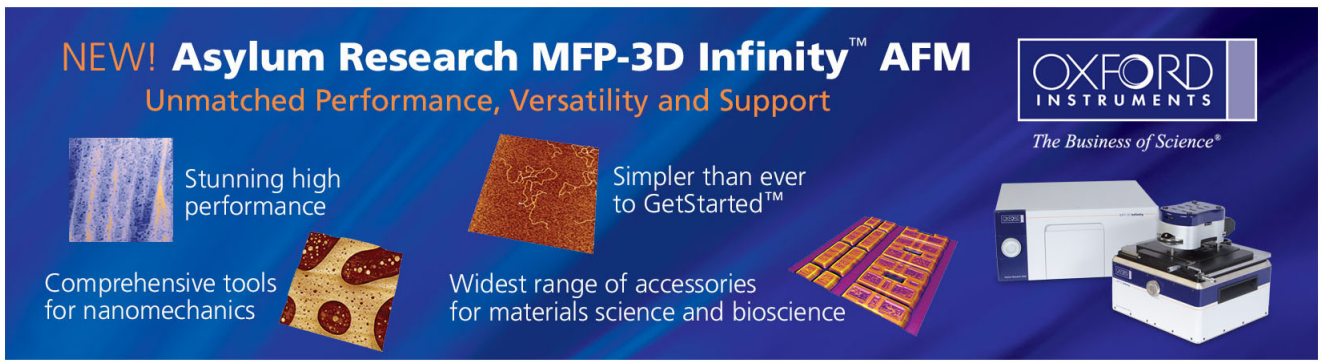

Surface-bound-exciton emission associated with domain interfaces in *m*-plane ZnO films

C. C. Kuo,[1] B. H. Lin,[1,2] Song Yang,[1] W. R. Liu,[2] W. F. Hsieh,[1,a)] and C.-H. Hsu[1,2,a)]
[1]*Department of Photonics and Institute of Electro-Optical Engineering National Chiao Tung University, 1001 University Road, Hsinchu 30050, Taiwan*
[2]*Division of Scientific Research, National Synchrotron Radiation Research Center, Hsinchu 30076, Taiwan*

(Received 30 January 2012; accepted 8 June 2012; published online 2 July 2012)

Small amount of $(10\bar{1}3)_{ZnO}$ domains were found in the *m*-plane ZnO films grown on *m*-sapphire by pulsed laser deposition, which provide strain relaxation of the *m*-ZnO matrix behaving as a low strain layer. Through carefully correlating low-temperature polarized photoluminescence spectra with the x-ray diffraction peak intensity ratio of $(10\bar{1}3)_{ZnO}/(10\bar{1}0)_{ZnO}$ of the samples grown at different temperature and after thermal treatment, we found that the broad-band emission around 3.17 eV may result from the interface defects trapped excitons at the boundaries between the $(10\bar{1}3)_{ZnO}$ domains and the *m*-ZnO matrix. The more $(10\bar{1}3)_{ZnO}$ domains in the *m*-ZnO layer cause the more surface boundary that makes the stronger surface-bound-exciton emission. And the *a*-axes of both the $(10\bar{1}3)_{ZnO}$ domains and the *m*-ZnO matrix are aligned with the *c*-axis of the sapphire (α-Al_2O_3) substrate. The *c*-axis of the $(10\bar{1}3)_{ZnO}$ domains rotates by about $\pm 59°$ against the common *a*-axis of the *m*-ZnO. © *2012 American Institute of Physics*. [http://dx.doi.org/10.1063/1.4732140]

ZnO, a wide-band-gap semiconductor with wurtzite structure, is a promising material for applications of ultraviolet (UV) light emitting devices (LED) and laser diodes (LD).[1–4] Due to its large exciton binding energy (60 meV), which can be further increased to 100 meV in quantum heterostructures,[5] stable excitons can exist at room temperature that offer the potential for making high-efficiency photonic devices. Usually, ZnO epi-layers grow preferentially with *c*-plane normal. In this orientation, ZnO consists of alternative layers of Zn cations and O anions along the growth direction that gives rise to a net spontaneous dipole field along the *c*-axis. ZnO-based LED and LD made of *c*-ZnO suffer from the quantum-confined Stark effect (QCSE) due to the piezoelectric and spontaneous polarizations.[6–8] To improve the quantum efficiency, devices with ZnO of non-polar orientations, such as *a*-plane $(11\bar{2}0)$ and *m*-plane $(10\bar{1}0)$, have been proposed. So far, the growth of high quality non-polar ZnO epi-layers is still far from being mature. For the *a*-ZnO grown on *r*-sapphire, recent studies showed that *a*-ZnO layers were subjected to significant anisotropic residual strain induced by the mismatches of lattice and thermal expansion.[9,10] The in-plane anisotropic strain leads to the change of crystal symmetry from wurtzite to orthorhombic. This symmetry transformation accounts for the observed distinct optical transition in polarized optical reflection and photoluminescence (PL) spectra.[10,11] These effects are the drawbacks if one is planning to design quantum wells for LED and LD. As to *m*-ZnO, previous works showed that it's difficult to grow high-quality ZnO epi-films with pure *m*-plane orientation. Domains with (0002) and $(10\bar{1}3)$ orientations often coexist with the major $(10\bar{1}0)$ oriented ones.[12,13] However, rare report on the epitaxial relationship of the extra domain with the m-ZnO matrix and no report, to the best our knowledge, correlating the existence of extra domain with the optical property of m-ZnO film. Therefore, in this study, we first determine the epitaxial relationship of the extra domain and the m-ZnO by x-ray diffraction (XRD) and evaluate the extra domain content from the peak intensity ratio of extra domain to m-ZnO. Determination of crystal axes of both the m-ZnO and extra domain is essential for investigating polarized PL with respect to the crystal structure. We observed a broad-band emission, which may result from the interface defects trapped excitons at the boundaries between the $(10\bar{1}3)_{ZnO}$ domains and the *m*-ZnO matrix, is strongly correlated the extra domain content.

ZnO films of thickness ~500 nm were grown on *m*-sapphire by pulsed laser deposition (PLD) using a KrF (248 nm) laser and a high purity (5N) ZnO target. During the deposition, substrate temperature was maintained at 400–600 °C. XRD measurements were performed with a four-circle diffractometer at the beamline BL13A of the National Synchrotron Radiation Research Center, Taiwan with incident wavelength of 1.0305 Å. Cross sectional transmission electron microscopy (TEM) images were recorded using a JEM-2100F TEM. Low-temperature photoluminescence (LT-PL) was performed at 13 K using a He-Cd laser at 325 nm as the pump source. Polarization dependent PL was conducted by using a Triax-320 spectrometer equipped with a UV-sensitive photomultiplier tube and a UV polarizer with pass band ranging from 280 to 400 nm.

Figure 1(a) illustrates the typical scattered intensity distribution of a XRD radial scan along surface normal. Pronounced diffraction peaks of ZnO $(10\bar{1}0)$, $(20\bar{2}0)$, $(30\bar{3}0)$, and sapphire $(30\bar{3}0)$ reflections confirm the *m*-plane orientation of the ZnO film. In addition, a broad shoulder at ~41.8°, close to the angular position of ZnO $(10\bar{1}3)$ reflection, indicates the possible existence of extra domains with $(10\bar{1}3)$ normal. On the other hand, the azimuthal scan across the *m*-ZnO off-normal $\{1\bar{1}00\}$ reflections, depicted in the inset of Fig. 1(a), shows two sets of peaks rotating 90° from each other. The intense pair with their angular positions

a)Authors to whom correspondence should be addressed. Electronic mail: wfhsieh@mail.nctu.edu.tw and chsu@nsrrc.org.tw.

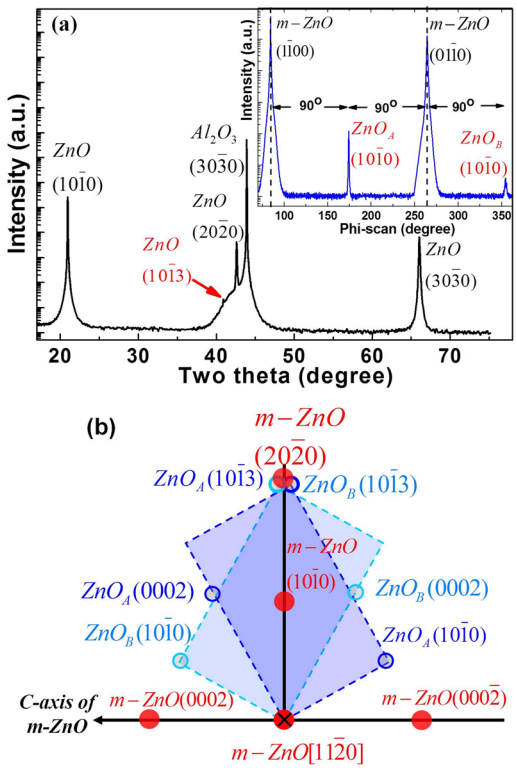

FIG. 1. (a) XRD radial scan along surface normal. An azimuthal scan across *m*-ZnO {1$\bar{1}$00} off-normal reflections is shown in the inset. The angular positions of sapphire {0006} reflections are marked by dashed lines as a reference. (b) A schematic of the diffraction pattern plotted along the $[11\bar{2}0]_{ZnO}$ zone axis. The Bragg reflections associated with the *m*-ZnO matrix and $(10\bar{1}3)_{ZnO}$ domains are depicted by red solid-circles and blue hollow-circles, respectively. Two $(10\bar{1}3)_{ZnO}$ domains share the same $[11\bar{2}0]_{m-ZnO}$ axis with the *m*-ZnO matrix but are rotated by ±59° around the $[11\bar{2}0]_{ZnO}$ axis, respectively.

coinciding with those of sapphire {0006} reflections are the (1$\bar{1}$00) and (01$\bar{1}$0) reflections of the *m*-ZnO layer, manifesting the $(10\bar{1}0)[11\bar{2}0]_{ZnO}||(10\bar{1}0)[0001]_{sapphire}$ epitaxial relationship. The two weak peaks are attributed to the (10$\bar{1}$0) reflections originating from two extra (10$\bar{1}$3)-oriented domains, whose [10$\bar{1}$3] axes are titled away from the surface normal by ∼1° toward the ±c-axis of the *m*-ZnO layer, respectively. This ∼1° tilting may easily lead to the missing of the $(10\bar{1}3)_{ZnO}$ domains if judging from the commonly performed $\theta - 2\theta$ scan alone.

After further analysis, we found the $(11\bar{2}0)$ planes of the *m*-ZnO matrix and the (10$\bar{1}$3)-oriented domains are parallel to each other. The relative orientations of the ZnO domains relative to the sapphire substrate are illustrated in Fig. 1(b). Judging from the content of $(10\bar{1}3)_{ZnO}$ domains and structural perfection of the *m*-ZnO matrix, we found the structural quality of the ZnO layers depends on the growth temperature; the sample grown at 500 °C exhibits the best structure properties among the samples studied. The lattice constants of both the *a*- and *c*-axes of *m*-ZnO and $(10\bar{1}3)_{ZnO}$ domains derived from the XRD data are much less than 1% of the bulk values, showing small strains; the $(10\bar{1}3)_{ZnO}$ domains show the free strain within 0.12%. The existence of $(10\bar{1}3)_{ZnO}$ domains that behaves as a strain free provides space for strain relaxation of the *m*-ZnO matrix.

By comparing the XRD peak intensity of the near specular $(10\bar{1}3)_{ZnO}$ reflection of the $(10\bar{1}3)_{ZnO}$ domains and the specular $(10\bar{1}0)_{ZnO}$ reflection of the *m*-ZnO matrix, with the structure factor taken into account, we estimated the intensity ratio of $(10\bar{1}3)_{ZnO}/(10\bar{1}0)_{ZnO}$ to be less than 3.8×10^{-4}. Moreover, its content depends on the growth temperature; the sample grown at 500 °C has the least $(10\bar{1}3)_{ZnO}$ content.

We also took cross-sectional TEM images under various geometries. A bright-field (BF) micrographs of the sample grown at 600 °C, which has a relatively high $(10\bar{1}3)_{ZnO}$ domain content, recorded along the ZnO [0002] zone axis is shown in Fig. 2. A selected area electron diffraction (SAED) pattern of the squared region near the *m*-ZnO/sapphire interface along ZnO $[11\bar{2}0]$ zone axis, shown in the inset, reconfirms the epitaxial relationship determined by XRD. In contrast to the higher $(10\bar{1}3)_{ZnO}$-domain content TEM image of the *m*-ZnO grown at 200 °C by MBE in Fig. 7 of Ref. 12, which shows the $(10\bar{1}3)_{ZnO}$ domain size of ∼50 nm having the XRD intensity ratio of $(10\bar{1}0)_{ZnO}/(10\bar{1}3)_{ZnO}$ of about 350, read from Fig. 3 of Ref. 12. It corresponds to the $(10\bar{1}3)_{ZnO}/(10\bar{1}0)_{ZnO}$ intensity ratio of $\sim 2.8 \times 10^{-3}$. No obvious feature associated with the $(10\bar{1}3)_{ZnO}$ domains is observed in our samples by both the BF TEM micrographs and the SAED patterns in Fig. 2 that manifests the relatively small size and low content of the $(10\bar{1}3)_{ZnO}$ domains. And the $(10\bar{1}3)_{ZnO}/(10\bar{1}0)_{ZnO}$ intensity ratio may be used as an indicator of the relative $(10\bar{1}3)_{ZnO}$-domain content.

It is well known that non-polar ZnO epi-films suffer from large density of stacking faults (SF).[13,14] High resolution TEM images of the *m*-ZnO/sapphire interface were taken along two orthogonal zone-axes to examine the structure defects of the samples. In Fig. 3(a), taken with the $[11\bar{2}0]_{ZnO}$ zone axis and diffraction vector $\vec{g} = [10\bar{1}0]_{ZnO}$, many basal stacking faults (BSF), marked by arrows, initiated from the ZnO/sapphire interface were identified. By contrast analysis, we found the BSFs belonging to intrinsic type-I_1 with a Burgers vector $\vec{b} = \frac{1}{6}[2\bar{2}03]$. The density of BSFs is estimated to be $5.7 \times 10^5 \text{cm}^{-1}$, similar to what reported in other works.[15,16] The micrograph recorded along $[0002]_{ZnO}$ zone axis with $\vec{g} = [11\bar{2}0]_{ZnO}$, shown in Fig. 3(b), reveals the highly perfect atomic arrangement of the ZnO layer. The inset shows the Fourier filtered image of the interface region. The nearly periodically arranged misfit dislocations, noted by extra half-planes inserted in the ZnO film, illustrate the domain matching epitaxial (DME) growth with four $(11\bar{2}0)_{ZnO}$ planes matching three $(0006)_{sapphire}$ planes along the $[1\bar{1}20]_{ZnO}$ direction and the DME growth has

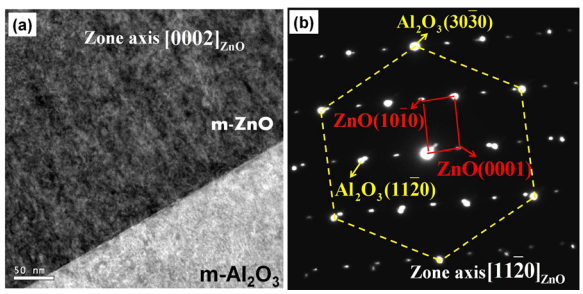

FIG. 2. A cross-sectional TEM bright field micrograph and a SAED pattern, shown (a) and (b), taken at the *m*-ZnO/saphire interface along the $[0002]_{ZnO}$ and $[11\bar{2}0]_{ZnO}$ zone axis. The lattices of *m*-ZnO and *m*-sapphire are marked, respectively, by solid and dashed lines.

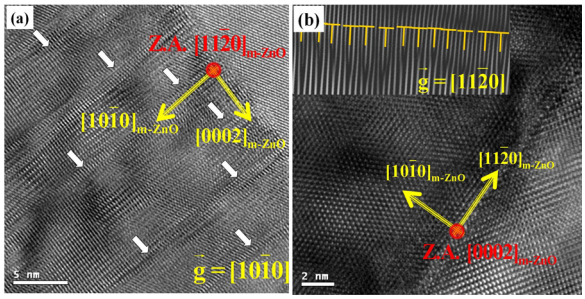

FIG. 3. The HRTEM micrographs taken along the (a) $[11\bar{2}0]_{ZnO}$ and (b) $[0002]_{m-ZnO}$ zone axis at *m*-ZnO/sapphire interface. The observed stacking faults in (a) were determined to be an intrinsic type-I_1 stacking fault. The inset in (b) shows a Fourier filtered image of a region at the interface where the misfit dislocations are marked by ⊥.

significantly reduced the lattice mismatch induced strain along this direction.

In order to investigate the influence of the $(10\bar{1}3)_{ZnO}$ domains to the optical properties of the *m*-ZnO epi-films, the LT-PL spectra taken at 13 K, shown in Fig. 4(a), of the samples grown at different temperatures were measured. The deep level emission centered around 2.2 eV, commonly known as the defect emissions attributed to the zinc interstitial or oxygen vacancies,[17–19] is negligible. Two dominant features are observed in the spectra: a sharp near-band edge (NBE) emission centered around 3.36 eV and a weak broadband one around 3.17 eV, noted as SX. The characteristic emission of ZnO BSFs is at 3.31 eV, whose shape similar to a gaussian has full width at half maximum (FWHM) around 7 meV at low temperature[20] that can be thus ruled out as the origin of the SX band. The intensity of the broad SX emission exhibits strong sample dependence and is positively correlated with $(10\bar{1}3)_{ZnO}$ domain content. This correlation is demonstrated by the variation of the XRD intensity of the $(10\bar{1}3)_{ZnO}$ reflection associated with the $(10\bar{1}3)_{ZnO}$ domains normalized to that of the $(10\bar{1}0)_{ZnO}$ reflection associated with the *m*-ZnO (stars) and the intensity of the SX emission normalized to the NBE emission (filled circles), shown in the inset of Fig. 4(a). The two curves show similar trend as a function of sample growth temperature. Moreover, thermal annealing of the 450 °C sample at 850 °C in 1 atm oxygen ambient for two hours significantly suppresses the SX band in the PL spectrum, depicted by the black curve in Fig. 4(a). It is accompanied by a more than 60% decrease of the XRD intensity of the reflections associated with the $(10\bar{1}3)_{ZnO}$ domains relative to that with *m*-ZnO. These observations obviously reveal that the origin of the SX band is related to the $(10\bar{1}3)_{ZnO}$ domains and thermal treatment effectively diminishes the $(10\bar{1}3)_{ZnO}$ domain content.

Because both the *m*-plane and $(10\bar{1}3)_{ZnO}$ oriented ZnO have the same crystalline structure with small strain, they are not expected to give rise to distinct PL features. The SX band is thus unlikely to originate from the $(10\bar{1}3)_{ZnO}$ domain itself. In light of the previous study of ZnO nanowires,

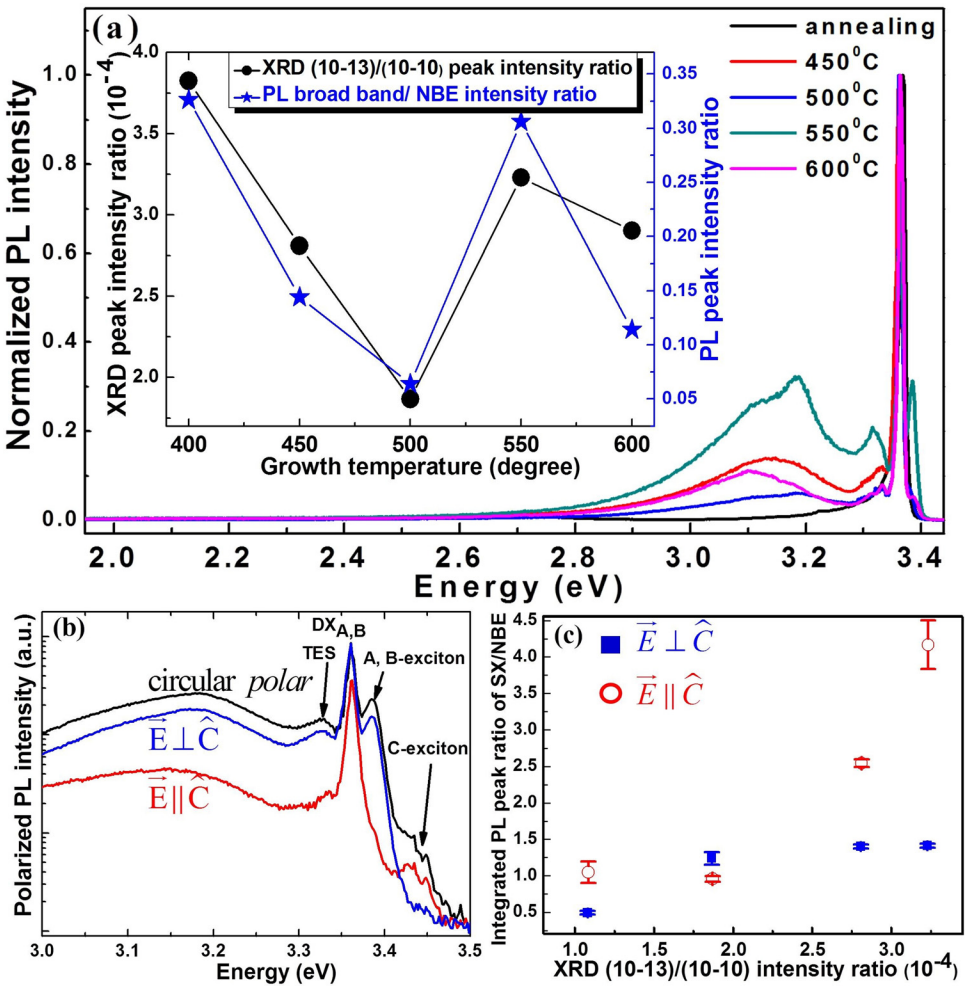

FIG. 4. (a) PL spectra of the samples grown at different temperatures recorded at 13 K show a strong NBE and a broad band emission without the deep level transitions. A spectrum of the sample annealed at 850 °C in O_2 is depicted by the black curve, where the SX band is suppressed. The insert in (a) shows the XRD intensity ratio of the $(10\bar{1}3)_{ZnO}$ reflection associated with the $(10\bar{1}3)_{ZnO}$ domains to the $(10\bar{1}0)_{ZnO}$ reflection of the *m*-ZnO (●) and the PL intensity ratio of SX/NBE (★) as a function of sample growth temperature. (b) The polarized spectra of the sample grown at 450 °C taken in various polarization configurations at 13 K and (c) the polarized PL peak (integrated) ratio of I_{SX}/I_{NBE} with different $(10\bar{1}3)_{ZnO}$ content.

Reparaz *et al.*[21] attributed the broad band in the PL spectra to the surface-bound exciton (SX) emission which shifted to the low energies accompanied by increasing emission intensity as the wire diameter decreased. The surface-bound states and defects localized in the interface between $(10\bar{1}3)_{ZnO}$ and $(10\bar{1}0)_{ZnO}$ regions may be responsible for the SX emission at 3.17 eV in this case.

We also compared the XRD $\theta-2\theta$ scans of the annealing and the as-grown samples and found the FWHMs of *m*-ZnO peaks decrease obviously after annealing. It is attributed to grain-size increase and strain relaxation. Note that the strains of the as-grown samples have already been much less than 1%. However, the FWHM of $(10\bar{1}3)_{ZnO}$ domains showing strain free according to the as-grown radius scan has slightly increased after annealing. With decreasing the $(10\bar{1}3)_{ZnO}$ domain content and grain size in *m*-ZnO epilayers by different growth conditions and thermal treatment, the diminished SX emission at 3.17 eV conspicuously results from reducing the surface-bound states attributed to the interface defects in Fig. 4(a).

To further examine the nature of the emissions, we performed polarized LT-PL measurements. Figure 4(b) illustrates the polarized LT-PL spectra of the 450 °C-grown sample and Fig. 4(c) shows the LT-PL peak ratio of I_{SX}/I_{NBE} dependent on the $(10\bar{1}3)_{ZnO}$ domains content with different polarized measurements. The exciton peaks located at 3.379, 3.388 and 3.443 eV are, respectively, attributed to free A-, B-, and C-excitons (FX_A, FX_B, and FX_C) in Fig. 4(b). The other NBE emission around 3.36 eV is originated from the neutral donor-bound excitons; the emission band at 3.33 eV is ascribed to the two-election satellite (TES) and phonon transition. It is known that the FX_A and FX_B are excited when the excitation polarization is perpendicular to the *c*-axis (E⊥c) of ZnO, whereas the FX_C is active when the polarization is parallel to the *c*-axis (E||c). According to the crystalline orientation determined by XRD, the E-field is perpendicular to the *c*-axes of both the $(10\bar{1}3)_{ZnO}$ and $(10\bar{1}0)_{ZnO}$ regions in the E⊥c geometry and thus the FX_A/FX_B emission is pronounced but the FX_C is not visible. In the E||c geometry, the E-field is parallel to the *c*-axis of *m*-ZnO but has a component of sin(χ), where $\chi\sim59°$ is the angle made between the *c*-axes of the *m*-ZnO and $(10\bar{1}3)_{ZnO}$ domains, projected onto the $[10\bar{1}0]$ axis of the $(10\bar{1}3)_{ZnO}$ domains. Therefore, in additional to the FX_C emission mainly coming from the *m*-ZnO, there exist a tiny bump at 3.379 eV corresponding to the FX_A/FX_B emission from the $(10\bar{1}3)_{ZnO}$ domains, whose weak intensity again reveals the small content of the $(10\bar{1}3)_{ZnO}$ domains. The relative intensities of the FX emissions confirm the much larger absorption cross-sections of the FX_A/FX_B than the FX_C.

To confirm the SX emission is correlated with the content of $(10\bar{1}3)_{ZnO}$ domains, we compared the peak (integrated) ratio (I_{SX}/I_{NBE}) of SX to NBE emissions under different polarization excitations with the XRD intensity ratio of $(10\bar{1}3)_{ZnO}/(10\bar{1}0)_{ZnO}$ in Fig. 4(c). We found the increase in I_{SX}/I_{NBE} as increasing $(10\bar{1}3)_{ZnO}/(10\bar{1}0)_{ZnO}$ is shown for the E||c excitation, but is insensitive for the E⊥c excitation. Because both the *m*-ZnO matrix and $(10\bar{1}3)_{ZnO}$ domains being excited through both FX_A and FX_B transitions contribute strong NBE and SX emissions due to the large absorption cross-sections for these two domains for the E⊥c excitation, the value of I_{SX}/I_{NBE} is insensitive to variation of the $(10\bar{1}3)_{ZnO}/(10\bar{1}0)_{ZnO}$ or the content of $(10\bar{1}3)_{ZnO}$ domains. For the E||c excitation, the *m*-ZnO matrix excited the FX_C transitions was shown less NBE emission, the $(10\bar{1}3)_{ZnO}$ domains still existed partial higher absorption cross-sections of the FX_A/FX_B. The higher ratio of I_{SX}/I_{NBE} with the higher $(10\bar{1}3)_{ZnO}$ domains content and on the E||c condition shown the larger ratio of I_{SX}/I_{NBE} result from the mainly SX emission attributed to the surface boundary in interface between $(10\bar{1}3)_{ZnO}$ domains and *m*-ZnO matrix. In this scenario, the PL peak ratio of I_{SX}/I_{NBE} reflects the probability of observing surface trapping emission and is consequently proportional to the boundary between $(10\bar{1}3)_{ZnO}$ domains and *m*-ZnO matrix which is positively correlated with the $(10\bar{1}3)_{ZnO}$ domain content. The much higher I_{SX}/I_{NBE} in the E||c geometry should be related to the higher binding efficiency of excitons to the interfacial states originated from the $(10\bar{1}3)_{ZnO}$ domains due to the larger surface-to-volume ratio and smaller size of the $(10\bar{1}3)_{ZnO}$ domains.

In conclusion we have grown non-polar *m*-plane ZnO on the *m*-sapphire substrate by PLD. XRD results reveal the presence of small amount of $(10\bar{1}3)$-oriented domains in the *m*-ZnO matrix. The peak positions of the free A-, B-, and C-exciton emissions in the PL spectra are close to that of bulk ZnO as a result of the $(10\bar{1}3)_{ZnO}$-oriented providing the strain relaxation mechanism. The broad-band emission is attributed to the emission from the surface bound excitons which are captured in the boundaries between the *m*-plane and $(10\bar{1}3)$-oriented domains.

This work is partially supported by National Science Council of Taiwan under Grant Nos. NSC-99-2112-M-006-017-MY3 and NSC-100-2112-M-006-002-MY3.

[1]E. S. P. Leong, S. F. Yu, and S. P. Lau, Appl. Phys. Lett. **89**, 221109 (2006).
[2]S. Chu, M. Olmedo, Z. Yang, J. Kong, and J. Liu, Appl. Phys. Lett. **93**, 181106 (2008).
[3]J. H. Lim, C. K. Kang, K. K. Kim, I.-K. Park, D. K. Hwang, and S. J. Park, Adv. Mater. **18**, 2720 (2006).
[4]A. Tsukazaki, A. Ohtomo, T. Onuma, M. Ohtani, T. Makino, M. Sumiya, K. Ohtani, S. F. Chichibu, S. Fuke, Y. Segawa, H. Ohno, H. Koinuma, and M. Kawasaki, Nat. Mater. **4**, 42 (2005).
[5]T. Makino, Y. Segawa, M. Kawasaki, and H. Koinuma, Semicond. Sci. Technol. **20**, S78 (2005).
[6]P. Waltereit, O. Brandt, A. Trampert, H. T. Grahn, J. Menniger, M. Ramsteiner, M. Reiche, and K. H. Ploog, Nature (London) **406**, 865 (2000).
[7]C. Morhain, T. Bretagnon, P. Lefebvre, X. Tang, P. Valvin, T. Guillet, B. Gil, T. Taliercio, M. Tesseire-Doninelli, B. Vinter, and C. Deparis, Phys. Rev. B **72**, 241305 (2005).
[8]Y. Noel, C. M. Zocovich-Wilson, B. Civalleri, Ph. D'Arco, and R. Doversi, Phys. Rev. B **65**, 014111 (2001).
[9]G. Saraf, Y. Lu, and T. Siegrist, Appl. Phys. Lett. **93**, 041903 (2008).
[10]C. C. Kuo, W.-R. Liu, W. F. Hsieh, C.-H. Hsu, H. C. Hsu, and L. C. Chen, Appl. Phys. Lett. **95**, 011905 (2009).
[11]T. Koida, S. F. Chichibu, A. Uedono, T. Sota, A. Tsukazaki, and M. Kawasaki, Appl. Phys. Lett. **84**, 1079 (2004).
[12]J.-H. Kim, S. K. Han, S. I. Hong, S.-K. Hong, J. W. Lee, J. Y. Lee, J.-H. Song, J. S. Park, and T. Yao, J. Vac. Sci. Technol. B **27**, 1625 (2009).
[13]J. W. Lee, J.-H. Kim, S. K. Han, S.-K. Hong, J. Y. Lee, S. I. Hong, and T. Yao, J. Cryst. Growth **312**, 238 (2010).
[14]J.-M. Chauveau, P. Vennéguès, M. Laügt, C. Deparis, J. Zuniga-Perez, and C. Morhain, J. Appl. Phys. **104**, 073535 (2008).
[15]W.-L. Wang, C.-Y. Peng, Y.-T. Ho, S.-C. Chuang, and L. Chang, J. Vac. Sci. Technol. A **29**, 031001 (2011).

[16]S. K. Han, J.-H. Kim, S.-K. Hong, J.-H. Song, J.-H. Song, J. W. Lee, J. Y. Lee, S. I. Hong, and T. Yao, J. Cryst. Growth **312**, 2196 (2010).
[17]W.-R. Liu, B. H. Lin, S. Yang, C. C. Kuo, Y.-H. Li, C.-H. Hsu, W. F. Hsieh, W. C. Lee, M. Hong, and J. Kwo, CrystEngComm **14**, 1665 (2012).
[18]T. Onuma, S. F. Chichibu, A. Uedono, Y. Z. Yoo, T. Chikyow, T. Sota, M. Kawasaki, and H. Koinuma, Appl. Phys. Lett. **85**, 5586 (2004).
[19]L. W. Sun, H. P. He, C. Liu, Y. F. Lu, and Z. Ye, CrystEngComm **13**, 2439 (2011).
[20]M. Schirra, R. Schneider, A. Reiser, G. M. Prinz, M. Feneberg, J. Biskupek, U. Kaiser, C. E. Krill, K. Thonke, and R. Sauer, Phys. Rev. B **77**, 125215 (2008).
[21]J. S. Reparaz, F. Güell, M. R. Wagner, A. Hoffmann, A. Cornet, and J. R. Morante, Appl. Phys. Lett. **96**, 053105 (2010).